Available online at www.sciencedirect.com
SCIENCE DIRECT®
Journal of Catalysis 226 (2004) 171–182
JOURNAL OF CATALYSIS
www.elsevier.com/locate/jcat

Modification of acid supports by solid-state redox reaction Part II. Acid and catalytic properties

A. Hagen [a,b,*], E. Schneider [c], M. Benter [a], A. Krogh [a], A. Kleinert [c], F. Roessner [c]

[a] *Technical University of Denmark, Department of Chemistry/Interdisciplinary Research Center for Catalysis, Building 312, DK-2800 Kongens Lyngby, Denmark*

[b] *Risoe National Laboratory, Materials Research Department, Building 228, P.O. Box 49, DK-4000 Roskilde, Denmark*

[c] *Carl v. Ossietzky University Oldenburg, Institute of Pure and Applied Chemistry/Industrial Chemistry 2, D-26111 Oldenburg, Germany*

Received 12 February 2004; revised 14 April 2004; accepted 21 May 2004

Abstract

ZSM-5 and Y zeolites, γ-alumina, and silica modified by solid-state redox reaction with zinc, gallium, manganese, and iron were studied in the conversion of cyclohexane and the nonoxidative conversion of ethane. The catalytic behavior was related to acid properties characterized by temperature-programmed desorption of ammonia (TPAD).

Keywords: Solid-state redox reaction; Zeolite; TPAD; Ethane; Cyclohexane

1. Introduction

Ion-exchanged zeolites are interesting catalysts in a variety of reactions such as nonoxidative conversion of alkanes [1], selective reduction of NO [2,3], or alkylation reactions [4]. In this respect, supported cationic iron, zinc, gallium, and manganese species were investigated among other promoters.

The conventional method for the preparation of modified zeolites is ion exchange in aqueous solution. However, solid-state reactions have attracted attention because they have a number of advantages over the liquid-phase methods: large amounts of liquids can be avoided because dry powders of the precursors are mixed. The preparation time is considerably shortened as the treatment usually comprises heating the mixture only instead of refluxing for hours, filtration, and washing. In addition, a higher or even full exchange degree can be obtained with multivalent cations. In solid-state methods, usually metal salts or oxides are thoroughly mixed with acid supports and react under a thermal treatment [5–8].

Exemplary, looking at zinc-containing ZSM-5 zeolites, the solid-state reactions between ZnO and H-ZSM-5 [9] and between Zn and ZSM-5 zeolite [10] have been studied. In both systems, catalysts with the same catalytic activity in the nonoxidative conversion of ethane were obtained as compared with Zn-ZSM-5 zeolites prepared by conventional ion exchange. The underlying solid-state reactions leading to the active catalyst are expressed in Eqs. (1) and (2), respectively,

$$\mathrm{ZnO} + 2\text{H-zeolite} \rightarrow \mathrm{Zn^{(2+)}}\text{-(zeolite)}_2 + \mathrm{H_2O}, \quad (1)$$

$$\mathrm{Zn^{(0)}} + 2\text{H-zeolite} \rightarrow \mathrm{Zn^{(2+)}}\text{-(zeolite)}_2 + \mathrm{H_2}. \quad (2)$$

In a detailed study comprising a number of metals and supports, the solid-state redox reaction was studied recently [11]. The main results were that zinc metal reacted with protons of a number of supports, namely ZSM-5 and Y zeolites, silica (containing silanol groups), and γ-alumina, yielding zinc ions with similar coordination as in Zn-ZSM-5 prepared by liquid ion exchange. In addition to zinc, also gallium, manganese, and iron underwent the solid-state redox reaction with the supports listed above. The temperatures at which this process occurred were correlating with the melting points of the metals [11]. The supports used in that study covered a wide variety of acid properties: type, number, strength, and distribution. However, these parameters did not have a decisive effect on the solid-state redox reaction. On the other hand, it is well known that acid properties may play important roles in catalytic reactions. There have

* Corresponding author. Fax: +45 4677 5758.
E-mail address: anke.hagen@risoe.dk (A. Hagen).

0021-9517/$ – see front matter
doi:10.1016/j.jcat.2004.05.027

been applied a number of methods to characterize acid sites in solid catalysts, e.g., IR spectroscopy, NMR spectroscopy, calorimetry, and temperature-programmed desorption (TPD) of probe molecules [12]. Each method has its own characteristics and strengths to reveal the specific parameters that are of most interest. By using TPD, a distribution of sites with different strengths toward the probe molecule is obtained. Ideally, the molecule reacting in the test reaction is used as the interaction forces observed in the characterization should match those operating in the reaction. However, in order to obtain a general picture and to be able to compare different catalysts used in different reactions, there are some "standard" molecules preferred in TPD studies like ammonia and pyridine to probe acid properties.

In the present study, catalysts prepared by solid-state redox reaction were characterized by TPD of ammonia. The acid properties thus observed will be discussed in relation to the catalytic properties in the cyclohexane conversion and nonoxidative conversion of ethane. In the first reaction, dehydrogenation functions and Brønsted acid sites determine the product distribution among olefins (benzene), isomerization (methylcyclopentane), and cracking products. The nonoxidative conversion of ethane is very demanding concerning the active sites, e.g., state of zinc and its ratio to Brønsted acidic sites, and the structural properties of the support [1]. Consequently, the study covers a variety of supports with different structural and acid properties, namely ZSM-5 and Y zeolites, γ-alumina, and silica, in combination with gallium, zinc, manganese, and iron ions introduced by solid-state redox reaction.

2. Experimental

2.1. Catalysts

Commercial zeolite samples (H-ZSM-5, NH_4-ZSM-5, AlSiPenta (Si/Al molar ratio: 13.5); H-Y, NH_4-Y, Sued-chemie (Si/Al molar ratio: 2.75), SiO_2 (Aldrich Davisil), and γ-alumina (LaRoche Industries. Inc.)) were used. The mixtures between metals (zinc (Riedel de Haën), gallium (Carl Roth), manganese (Riedel de Haën), and iron (Merck)) and support were prepared by grinding the two components in a ball mill for 4 h to give a metal content of usually 2 wt% (denoted as *Me* + *support*).

As reference sample, Zn-ZSM-5 zeolite was obtained by conventional threefold ion exchange of 5 g H-ZSM-5 zeolite with 25 mL of a saturated aqueous $Zn(NO_3)_2$ solution at 358 K for 5, 14, and 5 h. The final Zn content determined by back-exchange with ammonium acetate and subsequent complexiметric titration with EDTA was 2.4 wt%. The resulting powders were usually pelleted, crushed, and sieved to a particle size of 200–315 μm.

The solid-state redox reaction was initiated by a thermal treatment, called TPHE treatment (temperature-programmed hydrogen evolution, see also [11]): 0.5 g of the sample was heated in an argon flow of 60 mL/min first to 473 K, kept there for 2 h to remove physically adsorbed water, and then heated to 1123 K. The heating rates were 10 K/min.

2.2. Characterization

For temperature-programmed desorption of ammonia (TPAD), between 50 and 200 mg of the samples (all after TPHE treatment, including also the parent supports, 200–315 μm) was placed in a vertical glass-lined steel reactor. Prior to the experiment, the samples were dried in helium (50 mL/min) by heating with 8 K/min to 833 K and holding this temperature for 0.5 h. Ammonia was adsorbed at 333 K by feeding ammonia (2% in nitrogen, ca. 45–60 mL/min) through the reactor. A mass spectrometric detector and a NIR detector (MLT Analyzer, Rosemount Analytical) were used to control the composition of the gas outlet. The ammonia adsorption was stopped when the corresponding signal reached a constant value. The physisorbed ammonia was removed at 373 K by flushing with helium (50 mL/min). The temperature-programmed desorption was performed with a heating rate of 8 K/min in a 50 mL/min helium flow.

2.3. Test reactions

The conversion of cyclohexane was studied in a fixed-bed plug-flow microreactor. The chrome–nickel steel reactor was 300 mm long with an inner diameter of 3/8 inch. The amount of 0.5 g of the catalyst was placed over a stainless-steel mesh. The feed cyclohexane was evaporated in a saturator with magnetic stirrer at 353 K. The saturator was fitted with a glass condenser (318 K) through which the feed vapors were introduced to the setup with a constant flow of the nitrogen gas (20 mL/min). This flow was combined inside the setup with the carrier gas (50 mL/min nitrogen) giving a total molar flow of cyclohexane of 0.23 mmol/min. The catalyst was pretreated in situ at 823 K (10 K/min) in nitrogen for 2 h. The temperature was then adjusted to the desired value for the activity test (usually 673 and 773 K, respectively). All the connecting parts between the saturator, the reactor, and the on-line GC were electrically heated with heating tapes to avoid the condensation of hydrocarbons. The reactor outlet was coupled on-line to a HP 6890 GC gas chromatograph equipped with a 30 m HP-1 capillary column and a FID detector. The temperature program for product analysis was started at 318 K and after 6 min the temperature was increased to 378 K with a heating rate of 3 K/min. The quantification of the product composition was done based on the areas of the individual peaks after 115 min time on stream (on selected samples also initial values were given) and after taking into account the respective response factors for the individual components. Conversions and yields were thus calculated using the following equations:

$$X_{\mathrm{CH}} = \left(1 - \frac{A_{\mathrm{CH}} \cdot f_{\mathrm{CH}}}{\sum A_i \cdot f_i}\right) \cdot 100\%,$$

$$Y_P = \frac{A_P \cdot f_P}{\sum A_i \cdot f_i} \cdot 100\%$$

with

X_{CH}	Conversion of cyclohexane,
A_{CH}	Integrated peak area of cyclohexane,
f_{CH}	Response factor of cyclohexane = 1,
A_i	Integrated peak area of the component i,
f_i	Response factor of the component i,
Y_P	Yield of the product,
A_P	Integrated peak area of the product,
f_P	Response factor of the product.

The conversion of ethane was carried out in a plug-flow quartz microreactor. The sample (200 mg) was diluted with quartz (200 mg) of the same sieve fraction (200–315 µm). The pretreatment was done in helium at 823 K. To start the reaction, the reactant gas ethane and nitrogen (0.3 L/h each) were introduced at the reaction temperature of 823 K ($t = 0$). All lines between reactor outlet and GC were heated to 473 K to prevent condensation of hydrocarbons. The product stream was analyzed by an on-line coupled GC equipped with a 50 m PONA capillary column. The temperature was programmed from 233 to 493 K to ensure complete separation and elution of all product hydrocarbons from methane to dimethylnaphthalenes within about 25 min. The GC was equipped with both a thermal conductivity detector (TCD) and a flame ionization detector (FID) coupled in a row. CO_2 served as internal analytical standard, which was fed into the product stream after the reactor (0.03 L/h). Initial activities were calculated by extrapolating the conversion to $t = 0$. The molar conversions X of ethane were calculated from the FID signals using the 100% method

$$X = \frac{(n_{0,\text{ethane}} - n_{t,\text{ethane}})}{n_{0,\text{ethane}}} \cdot 100\%.$$

In addition, the conversions were calculated from the TCD areas of ethane and the standard CO_2. The agreement of these values was checked to deviate not more than ca. 10%.

Molar yields Y_x were obtained from FID areas using the 100% method and molar selectivities S_x were calculated according to

$$S_x = \frac{Y_x}{X} \cdot 100\%.$$

3. Results

3.1. Characterization of TPHE-treated samples by TPAD

In the TPAD experiment the acid properties of the formed metal–support composite were characterized after TPHE treatment, i.e., when the samples had already been heated in argon up to 1123 K prior to the adsorption of ammonia. In Figs. 1–3 the TPAD spectra of supports alone and with addition of the metals are shown. The amounts of chemisorbed ammonia are listed in Tables 1 and 2. Here, a distinction was made between the total amount and that desorbed at higher temperatures (between 773 and 833 K).

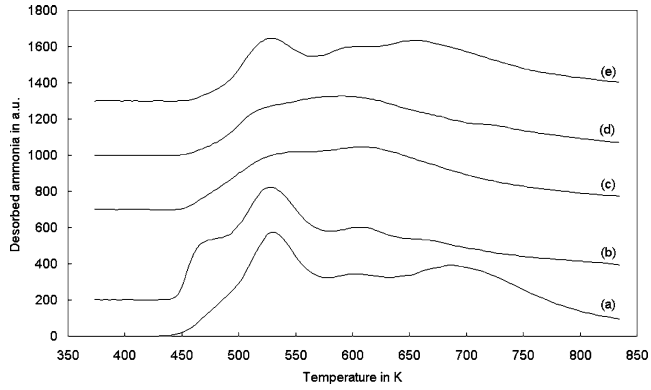

Fig. 1. TPAD spectra of H-ZSM-5 (a), Zn+H-ZSM-5 (b), Ga+H-ZSM-5 (c), Fe+H-ZSM-5 (d), and Mn+H-ZSM-5 (e), all samples after TPHE treatment.

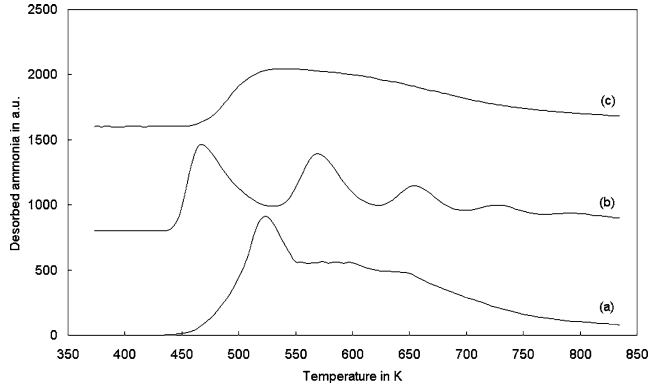

Fig. 2. TPAD spectra of H-Y (a), Zn+NH_4-Y (b), and Ga+H-Y (c), all samples after TPHE treatment.

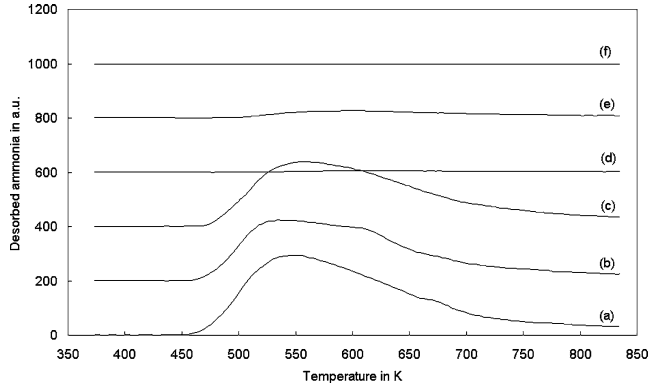

Fig. 3. TPAD spectra of γ-alumina (a), Zn+γ-alumina (b), Ga+γ-alumina (c), silica (d), Zn+silica (e), and Ga+silica (f), all samples after TPHE treatment.

The parent TPHE-treated H-ZSM-5 zeolite showed a low-temperature peak around 530 K. Furthermore, broad overlapping desorption peaks were observed in the high-temperature region (Fig. 1, curve a). The maximum for the peak at the highest temperature was 690 K. This spec-

Table 1
Amount of ammonia desorbed in the TPAD experiment on gallium and zinc-containing supports after TPHE treatment

(mmol/g)	ZSM-5 zeolite	Y zeolite	γ-Alumina	Silica
Parent				
Total	0.57	0.69	0.24	0.01
High temperature[a]	0.04	0.03	0.01	0.00
With 2 wt% Zn				
Total	0.62	0.53	0.20	0.07
High temperature[a]	0.07	0.04	0.01	0.01
With 2 wt% Ga				
Total	0.38	0.45	0.21	0.01
High temperature[a]	0.03	0.03	0.02	0.00

[a] Amount of ammonia desorbed between 773 and 833 K.

Table 2
Amount of ammonia desorbed in the TPAD experiment on iron and manganese-containing H-ZSM-5 zeolites after TPHE treatment

(mmol/g)	Fe+H-ZSM-5	Mn+H-ZSM-5
Total	0.34	0.41
High temperature[a]	0.03	0.04

[a] Amount of ammonia desorbed between 773 and 833 K.

trum changed drastically for Zn+H-ZSM-5 zeolite after TPHE treatment (Fig. 1, curve b). A new desorption peak in the low-temperature region appeared around 480 K. Further, a characteristic tailing toward higher temperatures was seen. The desorption line of the spectrum did not reach the base level, reflecting that ammonia was not completely desorbed up to temperatures of 833 K (Fig. 1, curve b). The TPAD spectra of Ga+H-ZSM-5, Fe+H-ZSM-5, and Mn+H-ZSM-5 (Fig. 1, curves c, d, and e) were quite similar to each other after TPHE treatment. The desorption features were smaller in intensity and broader compared to the parent zeolite. The TPAD spectrum of Mn+H-ZSM-5 zeolite showed at least distinguishable peaks around 530 and 660 K, which were similar to the metal-free H-ZSM-5 zeolite, whereas no distinct peaks were observed on the other two mixtures. There was no significant tailing of the curves toward higher temperatures as in the case of the zinc-containing ZSM-5 zeolite.

The amounts of desorbed ammonia were nearly the same on the parent H-ZSM-5 and the Zn+H-ZSM-5 zeolite both after TPHE treatment (Table 1). On all other metal-containing H-ZSM-5 zeolites, these amounts were much lower but comparable to each other (Tables 1 and 2). The amounts of ammonia being desorbed between 773 and 833 K decreased in the order Zn+H-ZSM-5 > H-ZSM-5 ≈ Ga+H-ZSM-5 ≈ Fe+H-ZSM-5 ≈ Mn+H-ZSM-5 (Tables 1 and 2). The highest amount on Zn+H-ZSM-5 reflects directly the tailing seen in the TPAD spectrum (Fig. 1, curve b).

The parent H-Y zeolite showed a similar TPAD spectrum as the parent H-ZSM-5 zeolite after TPHE treatment (Fig. 1, curve a and Fig. 2, curve a). There was also a distinct low-temperature peak around 520 K and several unresolved peaks with a maximum peak temperature of desorption at 640 K. However, the amount of desorbed ammonia was higher as in case of H-ZSM-5 zeolite. For the Zn+NH_4-Y sample (Fig. 2, curve b), in total about three distinct desorption peaks were observed after TPHE treatment. The low-temperature peak was at about the same temperature as on Zn+H-ZSM-5 zeolite (both ∼ 470 K). In contrast to the latter sample, however, there was no significant tailing observed toward higher temperatures (Fig. 1, curve b and Fig. 2, curve b). Ga+H-Y zeolite showed broad, low intensive desorption patterns without distinguishable single peaks (Fig. 2, curve c). The total amounts of desorbed ammonia decreased in the order H-Y > Zn+NH_4-Y > Ga+H-Y. The values for the high-temperature amounts were nearly the same (Table 1).

The TPHE-treated γ-alumina showed a broad TPAD spectrum with the maximum at about 550 K (Fig. 3, curve a). No significant changes in the spectrum after TPHE treatment of the support with zinc (Fig. 3, curve b) or gallium (Fig. 3, curve c) were observed. Both the total and the high-temperature amounts of desorbed ammonia were also very similar for these three samples. Generally, the values were significantly lower than those obtained on the corresponding zeolite samples (Table 1).

On TPHE-treated silica, no distinct desorption peaks were observed at all. The same applied for the zinc or gallium-containing TPHE-treated silica samples (Fig. 3, curves d, e, and f). The very low amounts of acid sites can also be inferred from the data in Table 1.

4. Conversion of ethane

Starting with the TPHE-treated ZSM-5 zeolite samples as shown in Table 3, the initial conversions of ethane obtained on H-ZSM-5, Fe+H-ZSM-5, and Mn+H-ZSM-5 were very low (below 1%). Interestingly, the values on metal ion-promoted H-ZSM-5 were even slightly lower than on the parent H-ZSM-5 zeolite itself. The highest initial conversion was observed on Zn+H-ZSM-5 zeolite followed by Ga+H-ZSM-5 zeolite.

Ethene and methane were formed on the TPHE-treated H-ZSM-5, Fe-ZSM-5, and Mn-ZSM-5 zeolites. In addition to these two products also aromatic hydrocarbons were observed on Ga+H-ZSM-5 and Zn+H-ZSM-5 systems.

The product selectivities plotted versus conversion also showed a different behavior for the gallium- or zinc-containing samples on one side and the iron- or manganese-containing zeolites and the parent H-ZSM-5 on the other (Figs. 4 and 5, respectively). On approaching zero con-

Table 3
Initial conversion of ethane on H-ZSM-5, Fe+H-ZSM-5, Mn+H-ZSM-5, Ga+H-ZSM-5, and Zn+H-ZSM-5 after TPHE treatment

H-ZSM-5+	Parent	Fe	Mn	Ga	Zn
Conversion (%)	0.5	0.3	0.3	2.3	13.6

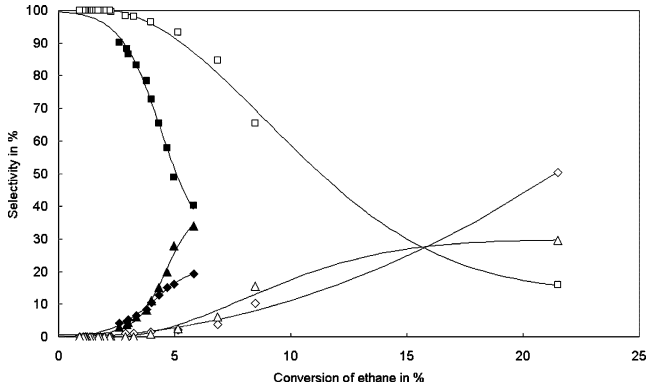

Fig. 4. Selectivities for the formation of ethene (squares), aromatic hydrocarbons (triangles), and methane (rhombs) on TPHE-treated Zn+NH_4-ZSM-5 (open symbols) and TPHE-treated Ga+NH_4-ZSM-5 (closed symbols) vs conversion of ethane.

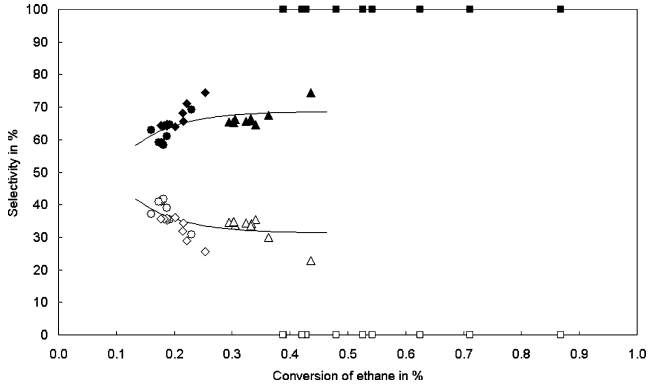

Fig. 5. Selectivities for the formation of ethene (closed symbols) and methane (open symbols) on H-ZSM-5 (triangles), Fe+H-ZSM-5 (rhombs), Mn+H-ZSM-5 (circles), and Zn+γ-alumina (squares) vs conversion of ethane, all samples measured after TPHE treatment.

version, the selectivities for the formation of methane and aromatic hydrocarbons approached zero for the first group. The selectivities for the formation of ethene, on the other hand, approached 100% (Fig. 4). In Fig. 5, the selectivities for the formation of methane and ethene are plotted versus the conversion for the TPHE-treated H-ZSM-5, and iron- and manganese-containing H-ZSM-5. It is difficult to judge whether methane or ethene rather tend to approach 100% at 0% conversion of ethane, although there seemed to be a slight increase for methane selectivity at the lowest observed conversions. For comparison, also the values obtained on TPHE-treated Zn+γ-alumina are shown (which behaved as the Zn+ZSM-5 samples when regarding the selectivity to methane and ethene though at lower conversion degrees), thus approaching 100% ethene selectivity and 0% methane selectivity at 0% conversion.

As there was almost no catalytic activity found on the iron- and manganese-containing H-ZSM-5 zeolites, the focus was set on gallium and especially zinc in the following experiments. In Fig. 6, the catalytic performances of zinc- or gallium-containing TPHE-treated samples are compared. The initial conversion of ethane was highest on zinc-

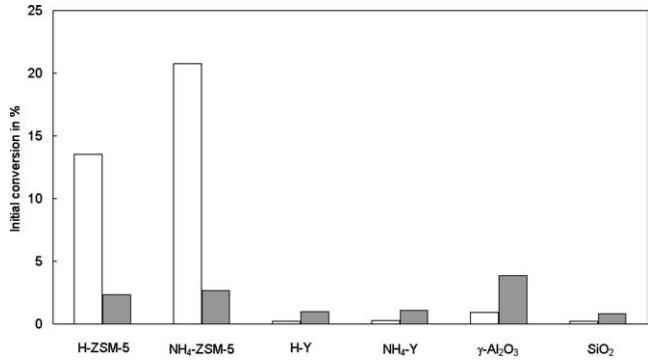

Fig. 6. Initial conversion of ethane on zinc-containing (white columns) and gallium-containing (gray columns) supports after TPHE treatment.

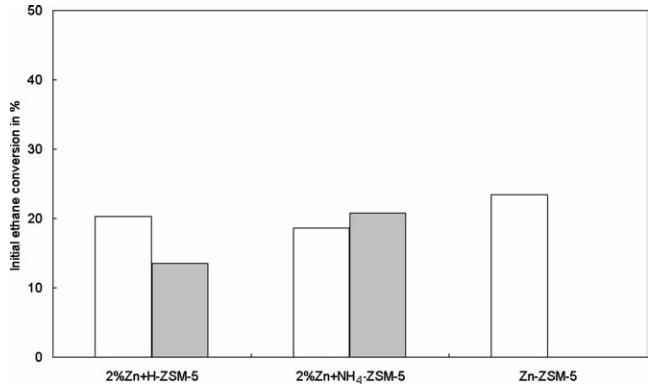

Fig. 7. Initial conversion of ethane on zinc-containing ZSM-5 zeolites before (white columns) and after (gray columns) TPHE treatment.

containing ZSM-5 zeolites whereas the gallium-containing counterparts had much lower activity. However, looking at the other supports, the conversions were always lower on the zinc- than on the gallium-containing materials. On both sample rows, ethene was the only product on the TPHE-treated mixtures with Y zeolites, γ-alumina, and silica. Aromatic hydrocarbons and methane were only found on the zinc- or gallium-containing ZSM-5 zeolites.

When the catalytic performances of the zinc-containing ZSM-5 zeolite samples are compared before and after TPHE treatment and with the Zn-ZSM-5 zeolite prepared by conventional ion exchange, there was almost no difference in the initial conversions of ethane as shown in Fig. 7. Only on the Zn+H-ZSM-5 sample after TPHE treatment a somewhat lower activity was observed. The product distributions on all zinc-containing samples compared at the same degree of conversion were the same (Table 4).

4.1. Conversion of cyclohexane

The conversion of cyclohexane was studied on zinc-containing samples comprising zeolites, γ-alumina, and silica. In addition, the zinc content was varied in the Zn+H-ZSM-5 zeolites.

To give a general picture of the catalytic test reaction, the conversions and product selectivities were plotted as a

Table 4
Molar product selectivities on zinc-containing ZSM-5 zeolites compared at 12% ethane conversion

Sample	Methane (%)	Ethene (%)	C_3/C_4 (%)	Aromatics (%)
Zn-ZSM-5	22.7	43.8	7.9	25.6
Before TPHE:				
2% Zn+H-ZSM-5	18.2	53.2	8.3	20.3
2% Zn+NH_4-ZSM-5	22.2	42.3	8.2	27.3
After TPHE:				
2% Zn+H-ZSM-5	17.0	45.1	8.5	29.4
2% Zn+NH_4-ZSM-5	16.5	53.1	8.7	21.7

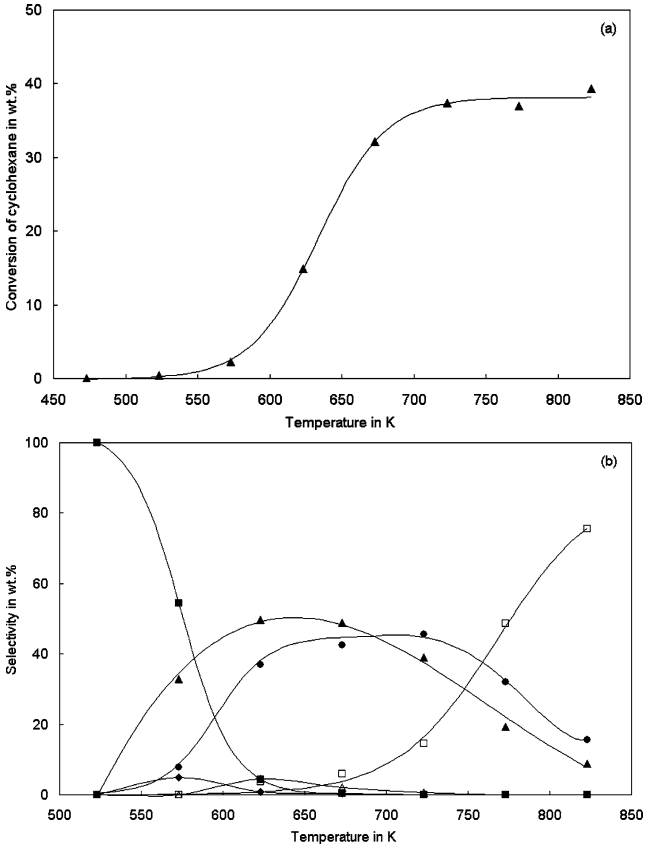

Fig. 8. (a) Conversion of cyclohexane and (b) selectivities for the formation of MCP (closed squares), C_1–C_3 hydrocarbons (closed triangles), C_4 hydrocarbons (open triangles), C_5 hydrocarbons (closed rhombs), C_{7+} aromatics (closed circles), and benzene (open squares) vs reaction temperature on Zn+NH_4-ZSM-5.

function of reaction temperature as obtained on a TPHE-treated Zn+NH_4-ZSM-5 zeolite sample. The conversion of cyclohexane increased with increasing temperature (Fig. 8a). The product distribution (Fig. 8b) can be divided into three regions. The first region between 523 and 573 K is characterized by a favored formation of methylcyclopentane (MCP), an isomerization product. Between 573 and 723 K formation of cracking products such as C_1–C_3 aliphatics and C_{7+} aromatics dominated. In the third temperature region between 723 and 823 K, benzene as a dehydrogenation product

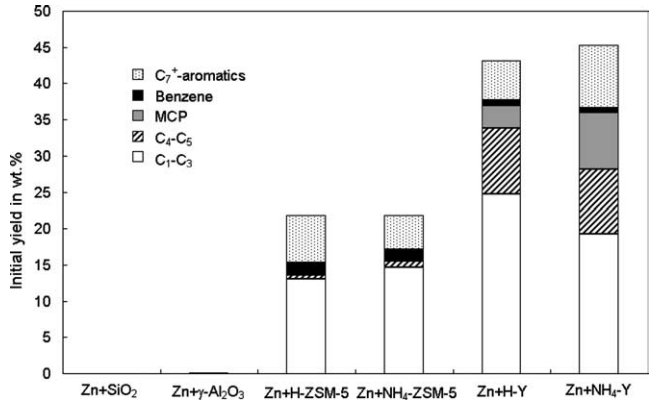

Fig. 9. Initial product distribution for the conversion of cyclohexane on Zn+SiO_2, Zn+γ-Al_2O_3, Zn+H-ZSM-5, Zn+NH_4-ZSM-5, Zn+H-Y, and Zn+NH_4-Y at 673 K.

appeared at the expense of the cracking products and alkylaromatics.

When screening all supports modified with zinc by solid-state redox reaction, the initial conversion of cyclohexane at 673 K increased in the order Zn+SiO_2 < Zn+γ-Al_2O_3 < Zn+H-ZSM-5 ≈ Zn+NH_4-ZSM-5 < Zn+H-Y ≈ Zn+NH_4-Y (Fig. 9). Initial values were chosen because the conversion decreased with time on stream, on the zinc-containing Y zeolites, in particular. On Zn+SiO_2 actually no products were found, whereas on Zn+γ-Al_2O_3, traces of benzene, C_6 hydrocarbons, and MCP were detected, but no cracking products. There was no large difference in the product distribution on the zinc-containing H- or NH_4-ZSM-5 zeolites. The same applied to the zinc-containing H- or NH_4-Y zeolite samples (Fig. 9). Comparing the product selectivities obtained on ZSM-5 and Y zeolites at the same degree of conversion, C_1 to C_3 aliphatics and aromatics were preferentially formed on zinc-free and zinc-containing ZSM-5 zeolites. C_1 to C_3 aliphatics and MCP formed the main part on the zinc-free and zinc-containing Y zeolites (Table 5). When following the selectivities as a function of conversion, that of benzene seemed to approach 100% at 0% conversion on the ZSM-5 zeolites, on both samples with and without zinc (Fig. 10), while on the Y zeolites, again with and without zinc, it was the selectivity for the formation of MCP (see Fig. 11).

The test reaction was now done using H-ZSM-5 modified with different amounts of Zn by means of solid-state redox reaction. For comparison, also the parent material and a Zn-ZSM-5 prepared by conventional ion exchange were studied. In addition, the reaction temperature was varied between 673 and 773 K. The conversion of cyclohexane decreased with increasing zinc content in the mixture Zn+H-ZSM-5, at the lower reaction temperature of 673 K, in particular (Fig. 12). There was a continually changing product spectrum in this row, too. At 673 K, C_1–C_3 cracking products and C_{7+} aromatics prevailed on H-ZSM-5 and Zn+H-ZSM-5 with lower zinc content, whereas benzene became prominent at higher zinc content and on the Zn-ZSM-5 zeolite

Table 5
Product selectivities on zinc-free and zinc-containing NH_4-ZSM-5 and NH_4-Y zeolites compared at 23 wt% cyclohexane conversion

	NH_4-ZSM-5	Zn+NH_4-ZSM-5	NH_4-Y	Zn+NH_4-Y
X in wt%	22.2	25.7	23.3	23.0[a]
S in wt%				
C_1–C_3	58.5	53.5	23.9	22.3
C_4	2.4	2.6	6.8	6.3
C_5	0.4	0.8	8.3	6.5
C_6	0.0	0.0	1.2	1.3
MCP	0.3	0.6	37.5	43.6
Benzene	4.1	4.2	1.9	1.6
C_7	0.0	0.0	1.1	1.0
Toluene	15.9	16.4	8.1	6.6
C_8-aromatic	15.8	16.5	8.5	7.8
C_9-aromatics	2.5	3.6	2.7	2.9
C_{10+}-aromatics	0.0	1.8	0.2	0.1

[a] Selectivity values were extrapolated to this conversion.

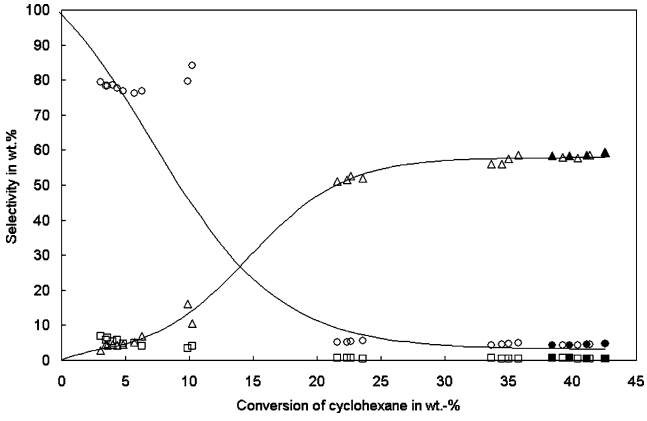

Fig. 10. Selectivities for the formation of MCP (squares), C_1–C_4 hydrocarbons (triangles), and benzene (circles) on Zn+H-ZSM-5 (open symbols) and H-ZSM-5 zeolite (closed symbols) vs conversion of cyclohexane.

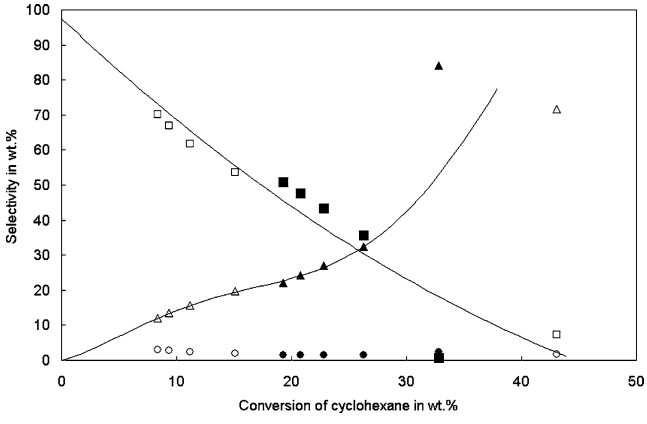

Fig. 11. Selectivities for the formation of MCP (squares), C_1–C_4 hydrocarbons (triangles), and benzene (circles) on Zn+H-Y (open symbols) and H-Y zeolite (closed symbols) vs conversion of cyclohexane.

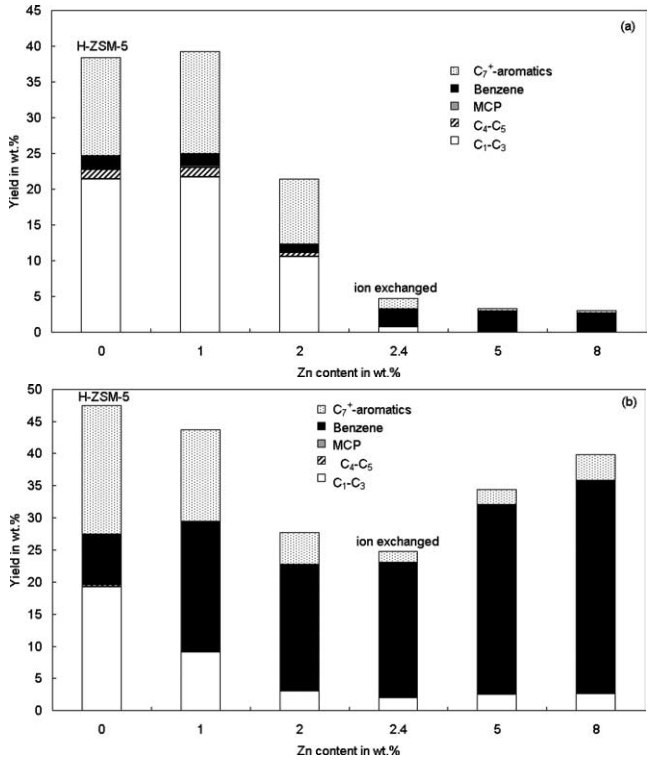

Fig. 12. Product distribution for the conversion of cyclohexane on Zn+H-ZSM-5 zeolites with different Zn contents (0, 1, 2, 5, and 8 wt%), and Zn-ZSM-5 (2.4 wt% Zn) at 673 (a) and 773 K (b) after 115 min time on stream.

(Fig. 12a). It must be noted that the amount of zinc supplied in the samples with 5 and 8 wt% exceeded the amount of Brønsted acid sites of the ZSM-5 zeolites (stoichiometric value 3.6 wt% zinc to give complete reaction of the Brønsted acid sites). Only small amounts of MCP were found and no C_6 aliphatics at all. At 773 K the following product distribution was observed. On the parent H-ZSM-5 zeolite, C_1–C_3 hydrocarbons and C_{7+} aromatics were still the main products, although benzene was formed to a higher extent as compared to 673 K. The cracking products were diminished to a low yield and the main product was benzene on the Zn+H-ZSM-5 samples, also on those with low Zn content (Fig. 12b).

5. Discussion

Recently [11] it was shown that the thermal treatment of mixtures consisting of metal and an acidic support results in the evolution of hydrogen accompanied by change of the coordination sphere of the metal. Particularly for zinc it was claimed that the formed ions occupy extraframework cationic position in the zeolites. Consequently, the change in the acidic properties, i.e., the change of the ratio Brønsted to Lewis sites, should also be reflected in the catalytic activity of the modified system. In order to gain information on the acidic properties of the samples modified by solid-state

redox reaction, temperature-programmed desorption of ammonia was applied.

When considering the parent supports ZSM-5, Y zeolite, γ-alumina, and silica, a broad range of acid properties is covered. All samples were studied after TPHE treatment, i.e., after previous heating up to 1123 K, in order to allow the direct comparison with the metal-containing catalysts after the same treatment. The results show, that the number of acid sites decreased in the order H-Y > H-ZSM-5 > γ-alumina > silica (see Table 1). This was not surprising from the common knowledge of these supports.

If one looks at the values for the zeolites, the amount of ammonia chemisorbed on H-ZSM-5 zeolite was lower than expected from the molar Si/Al ∼ 14, which would give rise to about 1 mmol/g acid sites. However, as the sample was subjected to the TPHE treatment before the TPAD measurement, the lower value for the amount of acid sites is not surprising. The difference amounting to 47% of the theoretic value should be due to dehydroxylation processes. Experimental evidence for this assumption was found in the TPHE studies as presented in [11]. The evolution of water could be seen at higher treatment temperatures (high-temperature peak) while following the ms signal at mass number 18.

Similarly, the number of acid sites found on the TPHE-treated H-Y zeolite was lower than the calculated values based on a molar Si/Al ratio of the material of ∼ 2.75. Accordingly about 65% of the hydroxyl groups were lost upon the TPHE treatment. As expected, the dehydroxylation effect was more pronounced in the case of the less stable Y in comparison to the ZSM-5 zeolites.

The TPAD spectra of H-Y and H-ZSM-5 zeolites (see Fig. 1, curve a and Fig. 2, curve a) showed the well-known shapes, indicating a distribution of acid sites with different strengths. The high-temperature peak of H-ZSM-5 zeolite is normally ascribed to ammonia adsorbed on strong Brønsted acid sites [13,14]. The broader features obtained on H-Y zeolite are a consequence of the distribution of acid sites with different strengths on this type of zeolite [13].

After TPHE treatment of the Zn+NH_4-Y zeolite, the TPAD characteristics changed in comparison to the parent zeolite. About three distinct desorption peaks appeared (see Fig. 2, curve b). Without attempting to assign each peak to a certain species this can be interpreted as zinc ions sited at different positions in the Y zeolite, whether these positions might be in the sodalite [15] or supercages [16,17]. In addition to zinc ions, also remaining hydroxyl groups acting as Brønsted acid sites contribute to the TPAD spectrum as shown previously by in situ DRIFT spectroscopy [11]. These acid sites should be reflected in the high-temperature region of the TPAD spectrum. The low-temperature peak can be assigned to the zinc sites, on the other hand, as the same desorption peak appeared first after the TPHE treatment both on the mixtures of zinc with Y and ZSM-5 zeolite (see Figs. 2 and 1, spectra a and b, respectively). This could be an indication that similar Zn species were formed, which, in turn, agrees very well with the results of Kazansky [18] who studied hydrogen adsorption on zinc-containing ZSM-5 zeolites and mordenites with varying Si/Al ratios. By the help of this probe molecule it was possible to distinguish between different cationic sites by evaluating DRIFT spectra. There was found a moderate red shift of the H–H stretching frequencies of H_2 adsorbed on Zn^{2+} in an aluminum-richer ZSM-5 zeolite, which was close to that for hydrogen adsorption on a Zn–Y zeolite [18]. Therefore it was suggested that the bivalent cations are localized in five- or six-membered rings of the zeolite framework housing two AlO_4 tetrahedrons per ring, both in the Y and in the aluminium-richer ZSM-5 zeolites.

Further, the TPHE-treated Zn+H-ZSM-5 zeolite sample showed a pronounced tailing toward higher temperatures. Ammonia was not completely desorbed up to a temperature of 833 K (Fig. 1, curve b). Previously, the same tailing was observed in the TPAD of Zn-ZSM-5 zeolites prepared by ion exchange and mixtures between ZnO and H-ZSM-5 zeolites after thermal treatment (where a solid-state ion exchange had taken place) as well [19]. As the appearance of the tailing was connected with the introduction of ionic zinc species, it was interpreted as interaction of ammonia with strong Lewis acid (cationic zinc) sites. While adsorbing hydrogen on silicon-rich zinc-modified ZSM-5 zeolites, Kazansky [18] found an unusual strong perturbation and heterolytic dissociation of molecular hydrogen to give new hydroxyl groups and zinc hydrides as concluded from the DRIFT bands. It was proposed that Zn^{2+} ions are located in the vicinity of one AlO_4 tetrahedron neutralizing the first positive charge. The remaining charge is compensated by electrostatic interaction with negatively charged tetrahedrons further away giving a larger distance between cation and basic framework oxygen and thus acid–base pairs with unusual catalytic properties [18]. In the case of ethane conversion, the ability of the zinc-containing ZSM-5 catalyst prepared by ion exchange or solid-state ion exchange to activate ethane was ascribed the strong acid sites found by TPD of ammonia and it is quite probable that these sites correspond to those proposed by Kazansky [18]. The presence of single Zn^{2+} cations was furthermore concluded by Biscardi et al. [20] who applied titration of ammonia to zinc-containing ZSM-5 zeolites.

When evaluating the acid properties and relating them to the activity in ethane conversion it is worth noting, that the test reaction is carried out at precisely those temperatures where there is still ammonia adsorbed on the zinc-containing ZSM-5 zeolites in the TPAD experiment. It is thus reasonable to assign and quantify strong acid sites to those where ammonia is desorbed from temperatures of 773 K upward (see Tables 1 and 2). The Zn+H-ZSM-5 zeolite after TPHE treatment showed the highest amount of “high-temperature” ammonia among all studied zeolites and cations and from the shape of the TPAD curve (see Fig. 1) it can be inferred that with further increasing the desorption temperature, this number would increase even more compared to the other samples.

In the nonoxidative conversion of ethane, only zinc-modified ZSM-5 zeolites showed appreciable activities among all metal species and supports (Fig. 6). It seems thus obvious that the activity could be related to these strong acid sites in the samples that desorbed ammonia above ∼ 800 K.

The acid properties, neither the entire number or number of strong sites as measured by TPAD, seemed to have that crucial effect on gallium-containing samples in the nonoxidative conversion of ethane. On gallium with ZSM-5 zeolites nearly the same initial conversion as on gallium with γ-alumina (2.4 and 3.8%, respectively) was seen, which was higher than for gallium on Y zeolites and gallium on silica (1 and 0.8%, respectively; Fig. 6). It is noteworthy that the values obtained on all zinc-containing supports (with the exception of the ZSM-5 zeolite) were all lower than on the corresponding gallium modified catalysts. When gallium- and zinc-modified samples are compared, higher conversions were only obtained on zinc-containing ZSM-5 zeolites, but all other gallium-containing samples were superior in activity (Fig. 6). This could be an indication for a higher intrinsic activity of gallium in that reaction, whereas zinc needs to be in the proper zeolitic, namely ZSM-5, environment to be active. One could also argue about the activity of gallium in different oxidation states (from +1 to +3) but such a distinction was not possible on the basis of the data obtained in this study.

The amount of acid sites found on iron and manganese-containing ZSM-5 zeolites was nearly the same as on the gallium-modified ZSM-5 samples (Tables 2 and 1). However, the initial conversion obtained on the former two catalysts was significantly lower (Table 3). Thus, it does not seems proper to relate the acid properties found by TPAD and catalytic activity in these cases.

When comparing the various metal ions on ZSM-5 zeolite it is also interesting to draw attention to the product distribution. There was a clear difference between zinc and gallium on one side and the parent ZSM-5 zeolite, iron, and manganese on the other. Though the slopes were different on TPHE-treated Ga+NH_4-ZSM-5 and Zn+NH_4-ZSM-5 when plotting selectivities vs conversion, the general trend was clearly visible: the amount of aromatic hydrocarbons and methane approached 0% at 0% conversion whereas ethene was the entire product at this point (Fig. 4). This points to ethene as primary product. Experimental evidence obtained previously by spectroscopic characterization and evaluation of catalytic properties [1] suggests that Lewis acid sites in Zn-containing ZSM-5 zeolites are the activating (electron withdrawing) species. Based on these facts and the results from [11] and this work, a simplified activation step can be formulated involving the scission of a C–H bond in ethane (Scheme 1). Another pattern or at least an additional one is likely to proceed on the other samples as the ratio between methane and ethene selectivity is higher by approaching 0% conversion (Fig. 5). Here one could also propose the formation of methane by scission of the C–C bond in ethane (Scheme 2). This path via a highly unstable transition

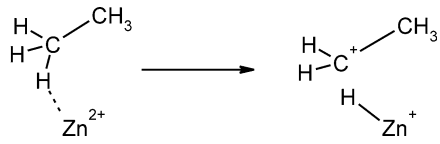

Scheme 1. Activation of ethane by C–H bond scission.

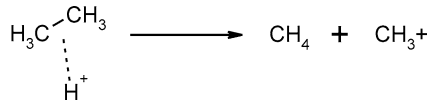

Scheme 2. Activation of ethane by C–C bond scission.

state is only valid on ZSM-5 zeolites but not on Y zeolites, γ-alumina, and silica as there was no methane formation at all.

In the conversion of ethane, zinc contributed by having Lewis acid properties. The conversion of cyclohexane as the other test reaction served to gain more information about the specific action of zinc in the samples prepared by solid-state redox reaction.

The general product distribution in the conversion of cyclohexane on zinc-containing samples was shown on Zn+NH_4-ZSM-5 as an example. There are clearly three different reactions proceeding in three different temperature regions reflecting their different activation energies. Isomerization was preferred at temperatures below 573 K. The key product of this path, MCP, prevailed in the product spectrum (Fig. 8b). The next reaction path occurring in the range between 573 and 723 K is cracking reflected by the formation of C_1 to C_3 cracking products. Finally, dehydrogenation is favored at temperatures above 723 K yielding benzene as the main product.

As in the case of ethane conversion, zinc-containing supports were studied in the conversion of cyclohexane, too, in order to reveal the function of acid sites and structure of the support in this type of reaction.

The catalytic performance in cyclohexane conversion was compared for H-ZSM-5 zeolites-containing different amounts of zinc. It must be noted that the theoretic value for a complete reaction of all Brønsted acid sites of the ZSM-5 zeolite is 3.6 wt% Zn. The first reaction temperature (673 K) lies in the range of favored cracking reactions on the H-ZSM-5 zeolites. The typical cracking product distribution combined with high conversion was observed on samples without zinc and up to 2 wt% zinc (Fig. 12). This is in line with results of Urda et al. [21] who postulated the cracking of cyclohexane as an initial step on Zn-ZSM-5 zeolites with lower zinc contents, whereas the dehydrogenation became more important only at higher zinc contents. One can therefore conclude that the Brønsted acid sites of the zeolite dominate the reaction network and that is of course also the case for a 2 wt% Zn sample where there are both Brønsted acid sites and zinc sites present. These two types of acid sites were found by in situ DRIFT spectroscopy and XANES as well [11]. The decrease of conversion with increasing content of zinc ions can be explained by the reduction of Brøn-

sted acid sites during the solid-state redox process. Since benzene was also detected on H-ZSM-5 zeolites its formation could be explained in term of hydride transfer during hydrocarbon conversion on acidic sites. However, if an amount of 5 wt% zinc is supplied, a complete consumption of all Brønsted acid sites to give zinc ions was reported previously [11]. These samples show a drastic change in catalytic behavior: (i) the conversion of cyclohexane dropped down and (ii) the main product became benzene (Fig. 12a) formed by dehydrogenation of cyclohexane on zinc species. The Zn-ZSM-5 zeolite prepared by conventional ion exchange does still contain Brønsted acid sites, which gave rise to the formation of small amounts of cracking products and higher aromatics. Thus, the presence of sufficient zinc ions is accompanied by a change of the reaction path of the ZSM-5 zeolite from cracking toward dehydrogenation. This strong preference of benzene formation was already observed previously in the nonoxidative conversion of ethane on zinc-containing ZSM-5 zeolites. In the absence of Brønsted acid sites, there was only benzene formation from the alkane; no cracking products or other higher aromatic hydrocarbons were formed [22]. Also in the conversion of cyclohexane, there is no cracking in a zeolite completely free of Brønsted acid sites as can be seen on the 5 and 8% Zn+H-ZSM-5 samples (see Fig. 12a). This reaction seems therefore to be sensitive to the ratio between Brønsted and zinc cations (Lewis acid sites) or at least to trace remaining Brønsted acid sites.

The same tendency was observed at a reaction temperature of 773 K. Generally, the conversion increased due to the higher temperature. The higher yield of benzene on the H-ZSM-5 zeolite indicates the faster hydride transfer as described above. This is a straight evidence for the fact that the dehydrogenation reaction has a higher activation energy compared with ring opening or isomerization reaction. The same conclusion was drawn by Wojciechowski and Zhao [23], who studied the reaction paths of hexyl ions on US-H-Y zeolite. The hydride transfer was thus much faster than the release of a proton from the intermediate carbenium ion at 673 K yielding more isomerization than dehydrogenation products. Further, a higher activation energy was found for the proton release, i.e., dehydrogenation compared to hydride transfer, i.e., isomerization [23]. Consequently, the dehydrogenation is increased at higher temperatures at the expense of isomerization. The presence of even small amounts of zinc drastically increases the direct dehydrogenation of cyclohexane on zinc species.

In order to clarify the influence of the nature of the support, the mixtures of zinc with Y zeolites, γ-alumina, and silica were studied. All samples were studied at a reaction temperature of 673 K, where cracking reactions prevail on the parent and a zinc-containing ZSM-5 zeolite as shown above. There was an increase of conversion in the order: $Zn+SiO_2 < Zn+\gamma\text{-}Al_2O_3 < Zn+H\text{-}ZSM\text{-}5 \approx Zn+NH_4\text{-}ZSM\text{-}5 < Zn+H\text{-}Y \approx Zn+NH_4\text{-}Y$. This order corresponds to the amount of acid sites as determined by TPD of ammonia for the parent material without zinc but not for the samples with zinc (see Table 1). From the results with varying zinc content in ZSM-5 zeolites (see above) it was concluded that as long as there are sufficient Brønsted acid sites, they would determine the reaction path toward cracking. To explain the results obtained on different zinc-containing supports, it would thus be helpful to distinguish between Brønsted acid sites and zinc ions acting as Lewis acid sites. This distinction was not possible on the basis of the TPD of ammonia experiments. However, from TPHE studies, in situ DRIFT spectroscopy, XANES results, and TPAD measurements presented in this work and [11], a distinction between those types is still possible. By subtracting the amount Brønsted acid sites that reacted with the submitted metallic zinc by solid-state redox reaction from the initial amount of the supports, the following order of remaining Brønsted acid sites in the zinc-containing TPHE-treated samples can be established: $Zn+SiO_2 < Zn+\gamma\text{-}Al_2O_3 < Zn+ZSM\text{-}5 < Zn+Y$. It is thus quite logical to explain the order of activity in the cyclohexane conversion by the amount of Brønsted acid sites, even in the presence of zinc cations in the samples. The fact that the TPD of ammonia yielded a higher total amount of acid sites on the Zn+ZSM-5 than on the Zn+Y zeolite could be due to the contribution of zinc cations acting as strong Lewis acid sites in the former sample.

Besides the activity, there was also a variation in the selectivities as a function of the support. On $Zn+\gamma\text{-}Al_2O_3$, isomerization as well as dehydrogenation products was found, although only in very low yields. This points to zinc inhabiting the dehydrogenation function and acid sites being responsible for the isomerization. However, there was no cracking, which can be explained by the absence of strong Brønsted acid sites as usually found in zeolites (vide supra).

The differences among the two studied zeolites become in particular obvious when the selectivities for the key products are compared at the same degree of conversion for the two zeolite samples and as functions of the conversions (Table 5, Fig. 10, and Fig. 11). Whereas MCP was formed on the Y zeolites in considerable selectivities, only traces were found on the ZSM-5 zeolites. This tendency was observed on both zinc-free and zinc-containing samples and points to two different mechanisms depending on the pore system of the zeolite. Moreover, when approaching 0% cyclohexane conversion, the selectivities for the formation of MCP seemed to approach 100% on the Y zeolites. On the ZSM-5 zeolites, however, this applied to the selectivity of benzene. These findings can be explained by taking into consideration the wide-pore system on Y zeolite (0.74 nm) in comparison to the narrower channels in ZSM-5 zeolites (0.56 nm). MCP is formed on both zeolites but in the narrow channel system of the ZSM-5 zeolite it is more difficult for the molecule to be transported outside and to desorb from the surface without further reaction. On diffusing to the outer surface the MCP will face acid centers and will be cracked. The consequence would be a low MCP content and no C_6 hydrocarbons in the product stream. On the Y zeolite, on the other hand, it is eas-

ier for the MCP to diffuse to the outer surface by making use of the wider pores. On diffusing to the outer side the MCP can undergo ring opening on acid sites. It is conceivable that the formed hexyl-carbenium ions dimerize to C_{12} carbenium ions in the wide-pore system of the Y zeolite followed by renewed cracking steps. This would explain the formation of C_5 and C_7 hydrocarbons on Y zeolite, a result that was also found while investigating the conversion of cyclohexane on a series of platinum-loaded H zeolites with varied pore-size distributions at elevated pressures of 13 bar [24].

There was no difference in the catalytic properties between the zinc-containing H or NH_4 forms of the zeolites (Fig. 9). It was shown previously [11] that the temperatures at which the solid-state redox reaction takes place is significantly lower on the NH_4 zeolite compared to the H zeolite. However, this different behavior did not reflect on the conversion of cyclohexane.

Summarizing the results obtained in the conversion of cyclohexane on zinc-free and zinc-containing zeolites, the following reaction scheme is presented for Y and ZSM-5 zeolites (Scheme 3). Starting from cyclohexane, zinc ions located at cationic positions act as dehydrogenation sites and favor the formation of benzene, though it is also produced to a low extent on the H zeolites by H-transfer processes (Scheme 3). On the wide-pore H-Y zeolite, MCP is produced, which then is further converted via ring opening, dimerization, and cracking. On the narrow-pore H-ZSM-5 zeolite, ring opening of cyclohexane and protolytic cracking on the strong Brønsted acid sites occur. Whether the ring opening proceeds via MCP or not was not cleared up. Finally, C_{7+} aromatics are formed by H-transfer processes from the C_1–C_7 hydrocarbons.

With increasing amounts of introduced zinc species the amount of benzene increases at the expense of cracking products because the number of Brønsted acidic sites is reduced. When the amount of supplied zinc is higher than the ion-exchange capacity of the ZSM-5 zeolite the dehydrogenation of cyclohexane dominates. Traces of cracking products could be a measure for remaining Brønsted sites not being involved in the ion-exchange process.

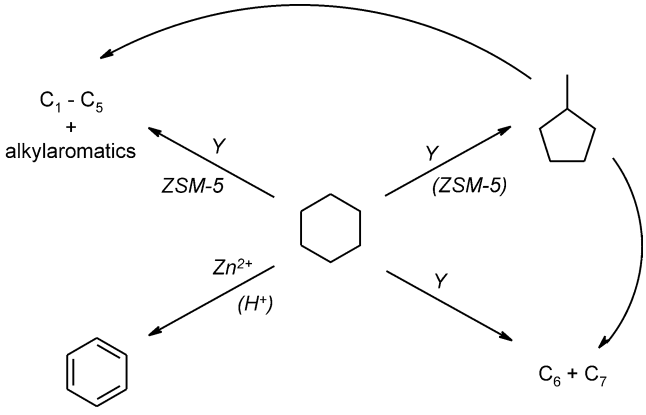

Scheme 3. Reaction paths in the conversion of cyclohexane.

6. Conclusion

The catalytic behavior of the acidic supports ZSM-5 and Y zeolites, γ-alumina, and silica modified with zinc, gallium, manganese, or iron by solid-state redox reaction in the conversion of ethane or cyclohexane did not depend on the total amount of acid sites measured by TPD of ammonia. On the other hand, nature and strength seemed to be determining parameters in this reaction. Zn+H-ZSM-5 zeolite possessed strong Lewis acid sites as found by TPD of ammonia. These sites are responsible for the activation of ethane and the formation of the initial product ethene, which in turn is further converted to oligomeric and, finally, aromatic hydrocarbons on the Brønsted acid sites of the zeolite. Gallium is less efficient on H-ZSM-5 zeolite than zinc but more active on the other supports: Y zeolite, γ-alumina, or silica. However, also the activity of these catalysts cannot be correlated to measured amounts of acid sites. Aromatic hydrocarbons were only found on the zinc- and gallium-containing ZSM-5 zeolites, not on the other supports or other promoters. Zinc and gallium gave rise to a mechanism starting with the formation of ethene, probably via C–H bond scission of ethane. H-ZSM-5 and manganese- and iron-modified H-ZSM-5 zeolites act probably as catalysts for the C–C bond scission in ethane to yield methane.

The conversion of cyclohexane was found to be a function of the amount of Brønsted acid sites in the samples, rather than the total amount as measured by TPD of ammonia, and the pore structure of the zeolite. The pore sizes of the zeolite determine whether MCP is initial product and able to leave the zeolite. The zinc sites direct the path toward direct dehydrogenation of cyclohexane avoiding the otherwise prevailing cracking path on the Brønsted acid sites. Thus, the conversion of cyclohexane is sensitive to the ratio of Brønsted acid to zinc sites in the zeolite.

Generally, the solid-state redox exchange of zinc with ZSM-5 zeolites generates the same catalytic centers as in the Zn-ZSM-5 zeolite prepared by ion exchange in aqueous solution.

Acknowledgments

The authors are grateful for financial support provided by the Deutsche Forschungsgemeinschaft in the frame of the *Priority program*: *From ideal to real systems*: *Bridging the pressure and materials gap in heterogeneous catalysis*. The work was supported by the IHP-Contract HPRI-CT-1999-00040/2001-00140 of the European Commission (Marie Curie Fellowship). The authors are thankful to S. Hagen for valuable assistance in the TPAD measurements and E. Symkowiak and L.D. Sharma for assistance in the conversion of cyclohexane test reaction during their guest stay in Oldenburg, Germany.

References

[1] A. Hagen, F. Roessner, Catal. Rev.-Sci. Eng. 42 (4) (2000) 403.
[2] N.W. Cant, I.O.Y. Liu, Catal. Today 63 (2000) 133.
[3] R.Q. Long, R.T. Yang, J. Catal. 207 (2002) 274.
[4] J.L. Sotelo, M.A. Uguina, J.L. Valverde, D.P. Serrano, Ind. Eng. Chem. Res. 32 (1993) 2548.
[5] H.K. Beyer, H.G. Karge, G. Borbély, Zeolites 8 (1988) 79.
[6] H.G. Karge, H.K. Beyer, G. Borbély, Catal. Today 3 (1) (1988) 41.
[7] H.G. Karge, G. Borbély, H.K. Beyer, G. Onyestyák, in: M. Philips, M. Ternan (Eds.), Proc. 9th Int. Congr. Catal., vol. 1, Chemical Institute of Canada, Ottawa, 1988, p. 396.
[8] G. Borbély, H.K. Beyer, L. Radics, P. Sandor, H.G. Karge, Zeolites 9 (5) (1989) 428.
[9] A. Hagen, F. Roessner, Stud. Surf. Sci. Catal. 83 (1994) 313.
[10] J. Heemsoth, E. Tegeler, F. Roessner, A. Hagen, Micropor. Mesopor. Mater. 46 (2001) 185.
[11] A. Hagen, E. Schneider, A. Kleinert, F. Roessner, J. Catal. 222 (1) (2004) 227.
[12] J.A. Martens, W. Souverijns, W. Rhijn, P.A. Jacobs, in: G. Ertl, H. Knözinger, J. Weitkamp (Eds.), Handbook of Heterogeneous Catalysis, vol. 1, Wiley–VCH, Weinheim, 1997, p. 324.
[13] C. Costa, J.M. Lopez, F. Lemos, F. Ramôa Ribeiro, J. Mol. Catal. A: Chem. 144 (1999) 221.
[14] N.-Y. Topsoe, K. Pedersen, E.G. Derouane, J. Catal. 70 (1981) 41.
[15] P.B. Peapples-Montgomery, K. Seff, J. Phys. Chem. 96 (1996) 5962.
[16] A. Seidel, B. Boddenberg, Chem. Phys. Lett. 249 (1996) 117.
[17] A. Seidel, G. Kampf, A. Schmidt, B. Boddenberg, Catal. Lett. 51 (1998) 213.
[18] V.B. Kazansky, J. Catal. 216 (2003) 192.
[19] F. Roessner, A. Hagen, U. Mroczek, H.G. Karge, K.-H. Steinberg, Stud. Surf. Sci. Catal. 75 (1993) 1707.
[20] J.A. Biscardi, G.D. Meitzner, E. Iglesia, J. Catal. 179 (1998) 192.
[21] A. Urda, G. Tel'biz, I. Sandulescu, Stud. Surf. Sci. Catal. 135 (2001) 4017.
[22] A. Hagen, F. Roessner, W. Reschetilowski, Chem. Ing. Technol. 18 (1995) 414.
[23] B.W. Wojciechowski, Y.-X. Zhao, J. Catal. 153 (1995) 239.
[24] G. Onyestyák, G. Pál-Borbély, H.K. Beyer, Appl. Catal. A 229 (2002) 65.